Applied Catalysis B: Environmental 92 (2009) 326–332

Contents lists available at ScienceDirect

Applied Catalysis B: Environmental

journal homepage: www.elsevier.com/locate/apcatb

Preparation of short, robust and highly ordered TiO_2 nanotube arrays and their applications as electrode

Yanbiao Liu, Baoxue Zhou *, Jinhua Li, Xiaojie Gan, Jing Bai, Weimin Cai

School of Environmental Science and Engineering, Shanghai Jiao Tong University, No. 800 Dongchuan Rd., Shanghai, China

ARTICLE INFO

Article history:
Received 16 June 2009
Received in revised form 30 July 2009
Accepted 4 August 2009
Available online 11 August 2009

Keywords:
TiO_2 nanotube arrays
Sonoelectrochemistry
Electron transport
Photoelectrocatalysis

ABSTRACT

The short, robust and highly ordered TiO_2 nanotube arrays (TNAs) electrode was prepared by sonoelectrochemical anodization of titanium in HF–H_2O electrolyte solution (referred as short TNAs, STNAs). The self-organized arrays of titania nanotubes of approximately 12–65 nm in diameter and 75–280 nm in length can be synthesized at anodic voltage of 5–20 V. The electron transport process within the STNAs electrode was much favorable in comparison with that for the long TNAs electrode synthesized by conventional magnetic agitation technique (referred as long TNAs, LTNAs), as confirmed by the obviously enhanced photocurrent response of STNAs electrode either in 0.02 M Na_2SO_4 electrolyte solution or in different concentrations of glucose solution or under different intensities of UV illumination. To investigate their photoelectrochemical applications, degradation of tetracycline, a typical pharmaceutical and personal care products (PPCPs), was carried out using photoelectrocatalytic (PEC) means, comparing with electrochemical (EC) and photocatalytic (PC) processes. The kinetic constant of the PEC process of STNAs electrode was ~3.17 times as high as its PC process. The color removal rate of tetracycline by STNAs electrode achieved 81% within 3 h, which was 21% higher than that for LTNAs electrode. In degrading tetracycline, 41% of TOC was mineralized using the STNAs electrode against 23% using LTNAs electrode under similar conditions. Such kind of titania nanotubes will have many potential applications in various areas as an outstanding photoelectrochemical material.

1. Introduction

Since the first discovery of photocatalytic water-splitting on a single-crystal TiO_2 electrode by Fujishima and Honda [1], extensive research [2–4] has shown that titania is a promising catalyst due to its low cost, unique structure, chemical inertness, remarkable properties and wide range of potential applications in degradation of organic pollutants, water-splitting, photovoltaic cells and other fields. A variety of preparation routes [5–7] have been used to fabricate nano-scaled TiO_2 of different geometric shapes and microstructures (i.e. wires, dots, particulates and tubes): anodic oxidation, hydrothermal synthesis, template synthesis, magnetic sputtering and sol–gel. Among these methods, anodic oxidation [5] is considered to be a simple and advantageous one for fabricating TiO_2 nanotubes film on Ti substrate directly. In 2001, Gong et al. [8] prepared highly ordered TiO_2 nanotube arrays (TNAs) by potentiostatic anodization of titanium in HF aqueous solution. This was followed by Macak et al. [9], Paulose et al. [10] and Prakasam et al. [11] by applying polar organic electrolytes, where the tube length can be further increased to several micrometers or even hundred micrometers. The nanotubular microstructures are perpendicular to the electrically conductive Ti substrate, forming a Schottky-type contact naturally and providing an unidirectional electric channel for the transport of photogenerated electrons [12,13]. Hence, the nanotube film reveals good charge separation and transport properties as well as elevated photoelectrical and electrochemical performances. For example, titania nanotube arrays based photoanodes have been reported perform as an excellent photoelectrocatalyst for various recalcitrant organic pollutants degradation [14,15], to improve the photosplitting of water [16], and been successfully used as photoanodes in dye-sensitized solar cells [16,17]. In our recent work [18,19], the TNAs-based chemical oxygen demand (COD) sensor can achieve rapid and accurate COD determination of wastewater.

The surface morphology structure of TNAs film is one of the most important factors affecting its photoelectrocatalytic (PEC) performance. The tube length of TNAs directly influence the electrons transport properties within the electrode material and the surface area of TNAs determines light harvesting performance of the electrode. The increase in tube length (or decrease in wall-thickness) favors the increment in the surface area of TNAs, which can improve the light harvesting capability of the electrode materials. However, the increase in tube length will also increase the transport resistance for photogenerated electrons and the

* Corresponding author. Tel.: +86 21 5474 7351; fax: +86 21 5474 7351.
E-mail address: zhoubaoxue@sjtu.edu.cn (B. Zhou).

0926-3373/$ – see front matter © 2009 Elsevier B.V. All rights reserved.
doi:10.1016/j.apcatb.2009.08.011

recombination rate between photogenerated charges. Literatures [12,19] have demonstrated that the increase in length of the nanotubes may not contribute positively to the PEC performance of the electrode materials and the short nanotubes prepared in inorganic electrolytes (i.e. HF–H_2O) was reported to possess enhanced photoelectrochemical properties contrarily. On the other hand, the increase in tube length will lead to the decreased mechanical stability of the electrode material. Yoriya et al. [20] found that the tube-to-tube binding, as well as the adhesion between the nanotube layer and the underlying substrate becomes weaker as the tube length increase. Meantime, the broken tubes and other debris from the organic anodization bath will readily to block the top surface of the nanotube film [10]. Therefore, the combination between nano-TiO_2 film and the substrate directly influencing the electrons transfer performance as well as the photochemical reactivity of the electrode materials.

It has been reported [21] that the sonoelectrochemical method (anodization under irradiation of ultrasonic wave) is an efficient technique for quickly synthesizing highly ordered and robust titania nanotubes. For example, Mohapatra et al. [22] utilized this method to prepare TNAs, ~650 nm in length, in H_3PO_4/KF electrolytes and, ~1 μm in length, in NH_4F/ethylene glycol electrolytes. In a typical anodization process, the composition of the electrolyte solutions directly affects the resulted tube length. Gong et al. [8] and our recent research [23] have reported the preparation of short nanotubes (~430 nm in length [23]) in HF-based electrolytes (i.e. HF–H_2O). However, no study has been reported to date regarding such sonoelectrochemical anodization route applied into HF-based electrolyte solutions to prepare even shorter nanotubes. In this work, we report on the preparation and characterization of short, robust and highly ordered TNAs by titanium anodization in HF–H_2O electrolytes under the irradiation of ultrasonic wave (referred as STNAs electrode), and compare the use of as-prepared STNAs with the nanotubes prepared by conventional magnetic agitation technique (referred as LTNAs electrode) in photochemical applications such as photocurrent response and organic compound degradation. The experimental results indicate that the STNAs electrode possesses excellent electrons transport properties and reveals obviously enhanced photochemical performance in comparison with LTNAs electrode.

2. Experimental

2.1. Materials

Titanium sheets (0.25 mm thick, 99.9% purity) were supplied by Kurumi Works (Japan). Hydrofluoric acid (HF ≥40 wt%), ethanol, acetone, sodium nitrate, sodium sulfate and glucose anhydrous (AR) were purchased from Sinopharm Chemical Reagent Company without further treatment prior to use. Tetracycline (>96.6%) was purchased from Wuhan Yuancheng Technology Development Co., Ltd. All solutions were prepared using high-purity DI water.

2.2. Preparation of STNAs

During a typical fabrication process of a short, robust and highly ordered STNAs film, titanium sheets, cut into samples of size 20 mm × 50 mm, were degreased by sonicating in 1:1 acetone and ethanol, followed by rinsing with DI water and dried in a stream of air. Electrochemical anodization of titanium was carried out using a DC power supply (TRADEX, 0–5 A, 0–60 V) to control the experimental current and voltage. The anodization experiments were carried out under ultrasonication irradiation (Kunshan Ultrasonic Instrument Co., Ltd.) at room temperature in 0.5 wt% HF solution using a platinum foil counter electrode (Figure S1, Supplementary Information). All the obtained STNAs, initially amorphous, needed to crystallize by annealing in air atmosphere for 3 h at 450 °C with heating and cooling rates of 1°/min (Figure S2, Supplementary Information).

2.3. Characterization of STNAs

The surface morphology of the as-prepared titanium oxide film was characterized with a field emission scanning electron microscope (PHILIPS, Netherlands, Sirion200). An X-ray diffractometer (BRUKER AXS-8 ADVANCE) was used to determine the crystalline structure of the samples.

2.4. Apparatus and methods

The PEC experiments were performed in a rectangular shaped quartz reactor (20 mm × 40 mm × 50 mm) using a three-electrode system with a platinum foil counter electrode, a saturated Ag/AgCl reference electrode and a TiO_2 work electrode. The supply bias and work current were controlled using a CHI electrochemical analyzer (CHI 660C, CH Instruments, Inc., USA). A 4 W UV lamp (GE, Japan G4T5) with central wavelength 254 nm was chosen as a UV light source. Light intensity was measured with a UV-irradiance meter (UV-B, Instruments of Beijing Normal University). The photocatalytic (PC) oxidation reaction was performed by using the same set-up without applying an external potential on the functional electrodes. The PEC degradation of tetracycline experiment was performed under the following conditions: UV irradiation (2.0 mW cm^{-2} light intensity), vigorous stirring, 0.5 V (vs. Ag/AgCl) of electric bias, pH 4.5, 0.02 M Na_2SO_4 as electrolyte, and no airflow. The initial concentration of tetracycline solution was 50 mg L^{-1} and the reaction solution was 25 ml during the experiment. The reaction solution (~3 ml) was quickly withdrawn at given reaction intervals, and was quickly returned to the reactor after being analyzed with a spectrophotometer (UV2102 PCS, UNICO, Shanghai) at 355 nm. A Multi-3000 total organic carbon analyzer (Analytik Jena, Germany) was employed to mineralization degree analysis of tetracycline solution.

3. Results and discussion

3.1. Preparation and characterization of STNAs

3.1.1. Current density–time curve

Fig. 1 presents the current density–time (I–t) curves for samples anodized in 0.5 wt% HF solution under ultrasonic wave irradiation

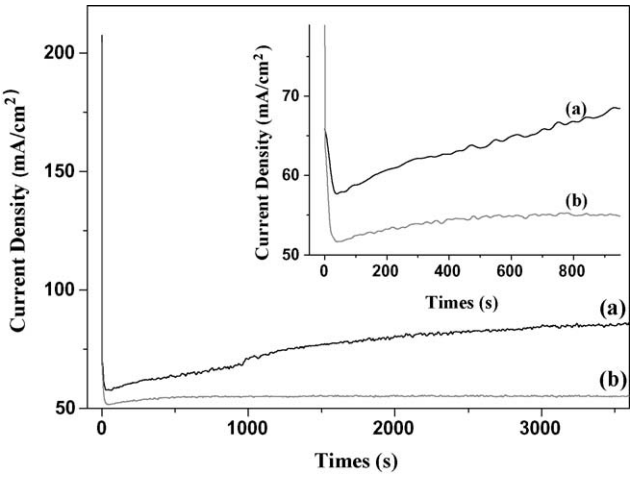

Fig. 1. Current density vs. time graph for Ti anodization in 0.5 wt% HF aqueous solution over 1 h period using (a) ultrasonic treatment and (b) magnetic stirring method.

(a) and magnetic agitation (b), respectively. It is evident that the two *I–t* curves reveals similar changing trend. The current density decreased sharply initially, followed by a rapid climbing. And then the current density keeps relatively stable, as can be seen from the inset in Fig. 1. During the initially current decay, this can be ascribed to the formation of TiO_2 barrier layer accompanied with the tremendous increase of resistance. In the following stage, the current density began to increase and keep growth due to the effect of the gradually enhanced electric-field assistant dissolution of titania, which decreased the surface resistance of the titanium substrate. In the third stage, the current density keeps relatively stable value since it reaches the maximum dissolution rate of titania at the bottom of nanotubes [8,23]. However, compared with the *I–t* curve under magnetic agitation (curve b), the current density under ultrasonic wave irradiation (curve a) was significantly improved and it takes longer time for the current density to achieve relatively stable value. Under the irradiation of ultrasonic wave, the significantly increased mass transfer leads to fast dissolution of TiO_2 layer, accompanied with the decrement of resistance of the Ti substrate as well as the increment in the current density. In this case, the dissolution rate of TiO_2 was much faster than the formation rate of TiO_2. Hence the current density obtained from the sonoelectrochemical anodization process was found to increase with time until a relatively equilibrium between the formation and dissolution of TiO_2 finally obtained at ~1800 s, which is much longer than the time needed to achieve a relatively equilibrium under magnetic agitation (~600 s).

The above processes can be ascribed to the interaction of the following two chemical reaction equations [8]:

$$Ti + 2H_2O - 4e \rightarrow TiO_2 + 4H^+ \quad (1)$$

$$TiO_2 + 6F^- + 4H^+ \rightarrow [TiF_6]^{2-} + 2H_2O \quad (2)$$

3.1.2. Effect of anodization time

To study the effect of anodization time on the microstructure of the as-prepared STNAs, a set of experiments were performed. The samples anodized under ultrasonic wave irradiation for different time intervals ranging from 10 s to 3600 s were monitored by taken field emission scanning electron microscope (FESEM) images, as given in Fig. 2. In the initial stage, within 10 s (Fig. 2a), some pits started to form on the surface of the titanium substrate. After 100 s (Fig. 2b), a continuous nanoporous layer emerges. A tube-like surface morphology was obtained over 500 s

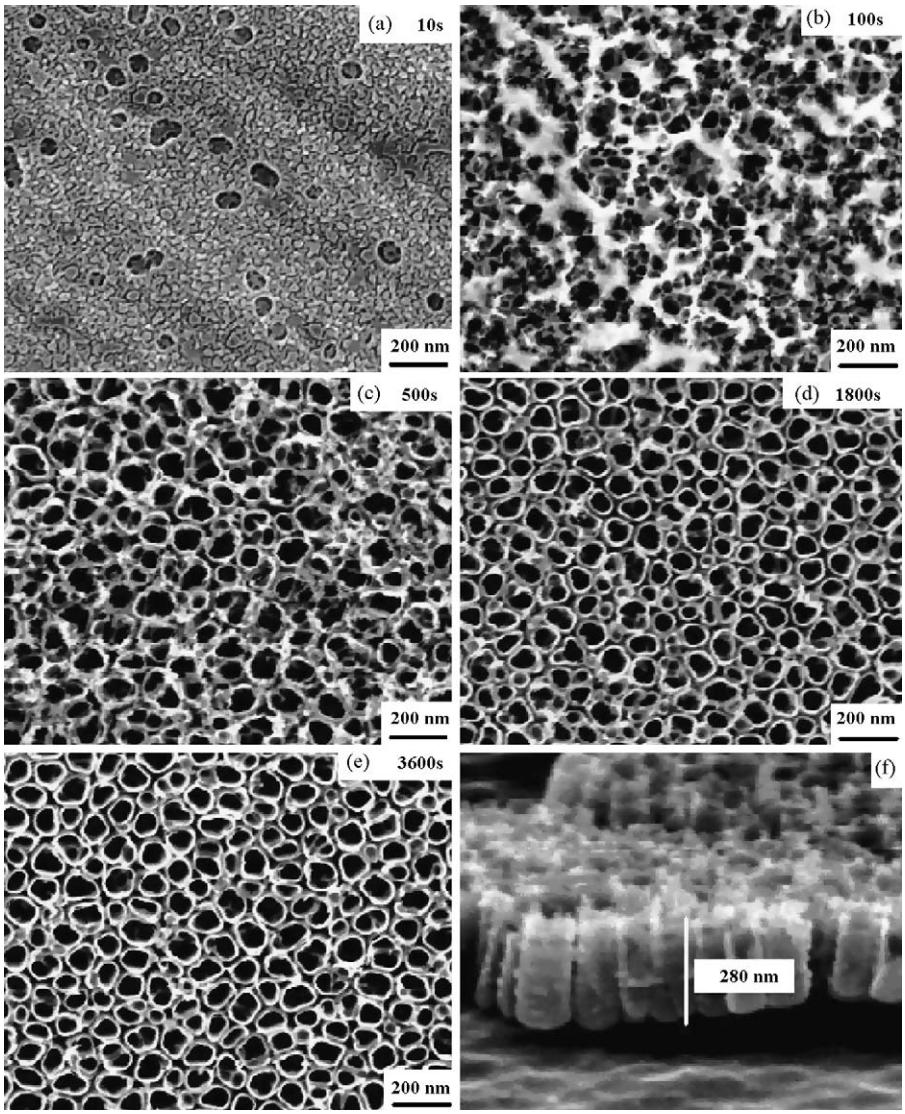

Fig. 2. FESEM images showing the different stages of STNAs film formation during anodization at 20 V in 0.5 wt% HF aqueous solution under ultrasonic waves irradiation (a–e) and (f) is cross-sectional view of (d), presenting the as-prepared nanotubes with a tube length ~280 nm.

Table 1
Dimensional data and roughness factor of TiO_2 photoanodes.

Photoanode	D (nm)	W (nm)	L (nm)	G
LTNAs	70 ± 3	15 ± 2	430 ± 20	27.5
STNAs	65 ± 2	5 ± 1	280 ± 10	26.3
TNPs[a]	220 ± 10	20 ± 2	27.5 ± 3	1.7

[a] As for TNPs, L is set as half the pore depth and W is half the average voids between two adjacent pores.

anodization (Fig. 2c), and after 1800 s the surface was completely filled with well-aligned nanotubes ~280 nm in length, ~65 nm in inner diameter and ~5 nm in wall-thickness (Fig. 2d and f). With further anodization (Fig. 2e), there is almost no further change in the nanotubular structure when anodization process extended from 1800 s to 3600 s. However, carrying out the above experiment under magnetic agitation for 1800 s at 20 V produced a nanotubular morphology ~430 nm in length, ~70 nm in diameter and ~15 nm in wall-thickness [23] (see Table 1). It is evident that the titania nanotubes prepared by sonoelectrochemical method feature short tube length and thin wall-thickness.

Sonoelectrochemistry works through the generation and subsequent destruction of cavitation bubbles and the collapse of the transient bubbles will cause a liquid jet on the surface of STNAs electrode, which could increase the dissolution rate of TiO_2 barrier layer during the formation of titania nanotubes. This effect increases the mass transfer through the nanotubular microstructure and thus accelerate the diffusion of F^- ions into the nanotubes and effusion of $[TiF_6]^{2-}$ ions from the nanotube layer [22]. Therefore, the resulted length and wall-thickness of the as-prepared STNAs film was obviously decreased compared with that obtained by magnetic agitation. Moreover, since the mass transfer throughout the anodization process is uniform under ultrasonic wave irradiation, the as-prepared STNAs film is short, robust and highly ordered.

The roughness factor, i.e. the physical surface area of the film per unit of projected area, measures the internal surface area of the electrode materials and is of crucial significance in photochemical applications such as photocatalysis or photoelectrocatalysis [24]. In a typical TNAs-based PC or PEC process, the amount of light harvested by the electrode film is directly related to the film roughness factor. Herein, assuming an idealized nanotubular structure of inner diameter D, wall-thickness W and tube length L, the purely geometric roughness factor of the nanotubes is calculated as [25]:

$$G = [4\pi L\{D + W\}/\{\sqrt{3}(D + 2W)^2\}] + 1 \quad (3)$$

The quantitative dimensional data and roughness factor of both TiO_2 photoanodes were given in Table 1. The roughness factor is 26.3 and 27.5, respectively, for STNAs electrode and LTNAs electrode. It is evident that the STNAs electrode possesses similar roughness factor value with the LTNAs electrode, although its tube length is much shorter. This can be ascribed to the thinner wall-thickness of STNAs electrode leads to more nanotubes packed together in per unit area. As a comparison, we also present the roughness factor value of a novel kind of TNPs electrode reported in our previous work [26], with low surface area, strong mechanical stability and obviously enhanced photoelectrochemical properties, in Table 1.

3.1.3. Effect of the applied potential

To investigate the influence of the applied potential on the microstructure of the as-prepared nanotubes under the presence of ultrasonication, a set of experiments were done with the anodic voltage varying from 5 V to 20 V by keeping the electrolyte composition and anodization time (1800 s) constant. Fig. 3 presents the tube diameter as well as the tube length of the resulted STNAs film changes with the applied potential. Anodization at 5 V for 1800 s only gives a thin layer of porous film (Figure S3, Supplementary information), while a 20 V anodization results a nanotubes layer with diameter and length of ~65 nm and ~280 nm, respectively. It is evident that both the tube diameter and the tube length increased with the increment in applied potential. However, a 40 V anodization for half an hour yielded films with a sponge-type appearance instead of the tubular structure (Figure S3, Supplementary information). Nanotubes of approximately 12–65 nm in diameter and 75–280 nm in length can be synthesized as the anodic voltage ranging from 5 V to 20 V. Therefore, one can control the resulted nanotube parameters by changing the anodization time and applied potential and further research is needed to find the optimum anodizing conditions to achieve optimal arrays of titanium oxide nanotubes.

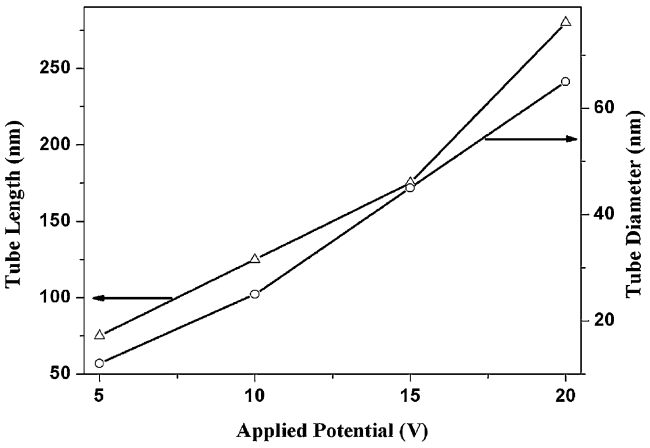

Fig. 3. Effect of applied potential on the tube diameter and length of the TiO_2 nanotubes synthesized by sonoelectrochemical anodization in 0.5 wt% HF aqueous solution for 0.5 h.

3.2. Photocurrent response

The photoelectrochemical properties of different electrode materials (see Table 1), were carried out by comparing their photocurrent response. Fig. 4 compares the photocurrent response of STNAs electrode (curve a) with LTNAs electrode (curve b) and TNPs electrode (curve c) in 0.02 M Na_2SO_4 solution as a function of applied potential under UV illumination (2.0 mW cm^{-2} light intensity). As can be seen that, the STNAs electrode reveals obviously enhanced photocurrent response compared with LTNAs

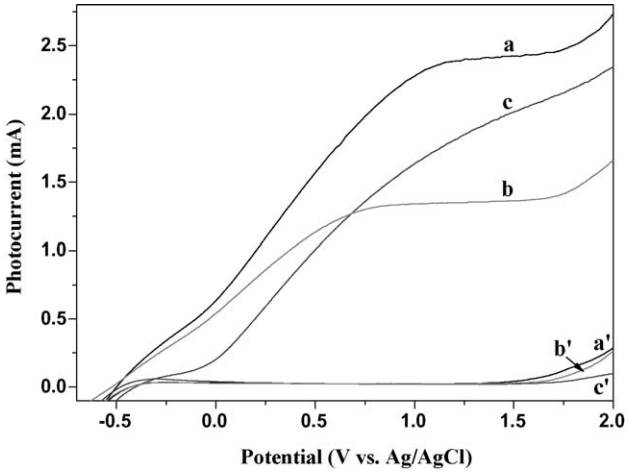

Fig. 4. Photocurrent vs. applied potential (vs. Ag/AgCl) in 0.02 M Na_2SO_4 under UV illumination for STNAs electrode (a), LTNAs electrode (b) and TNPs electrode (c), respectively. Dark current for the samples are shown in (a′), (b′) and (c′).

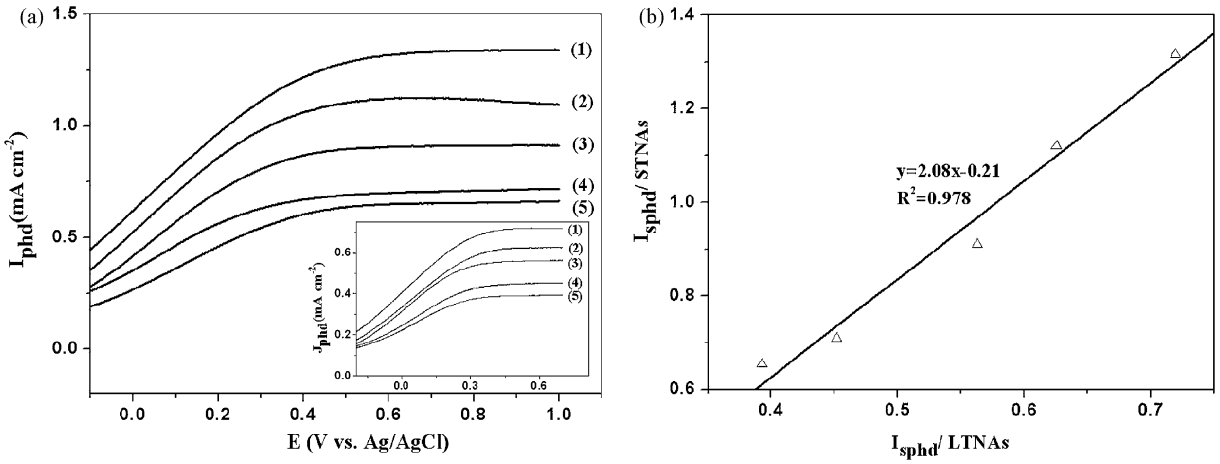

Fig. 5. (a) Voltammograms of STNAs electrode and LTNAs electrode (inset) obtained from a 0.1 M $NaNO_3$ blank and various concentrations of glucose at 4.7 mW cm^{-2} light intensity. The glucose concentration: (1) 10 mM, (2) 5 mM, (3) 1 mM, (4) 0.1 mM and (5) 0 mM. (b) The relationship between the saturated photocurrent density of STNAs electrode and LTNAs electrode at different concentrations of glucose solution.

electrode and TNPs electrode. At an applied potential of 1.2 V, the photocurrent for STNAs electrode is 1.80 and 1.32 times, respectively, as high as that for LTNAs and TNPs electrode. The observed dark current for all samples were found to be negligible, curve a′, b′ and c′. Although the roughness factor is ranked as: LTNAs ≈ STNAs ≫ TNPs, the photoelectrochemical reactivities were ranked as: STNAs > TNPs > LTNAs. This might mean the STNAs electrode possesses the best electrons transport properties and PEC performance compared with other two electrodes under given experimental conditions.

Fig. 5a illustrates typical voltammograms obtained from 0.1 M $NaNO_3$ solution containing different concentrations of glucose at the STNAs electrode and the LTNAs electrode (inset) under fixed UV illumination (4.7 mW cm^{-2} light intensity). In all the cases, the STNAs and LTNAs photoanodes exhibit similar photocurrent density–potential (I_{phd}–E) characteristics, even in the absence of organic compound (0.1 M $NaNO_3$ alone). This phenomenon is similar to those that reported by Jiang et al. [27]. As can be seen from Fig. 5a, the I_{phd} increased as the biased potential increased at low potentials, but subsequently became saturated at varying I_{phd}–E values. At a given potential bias, the saturated photocurrent density (I_{sphd}) increased as the concentrations of the glucose increased. While at a fixed concentration of glucose, the I_{sphd} value for STNAs electrode is found always higher than that for LTNAs electrode. Since the photocurrent directly reflects the photoefficiency of the photoelectrochemical system regardless of the type of organic compounds [27] and the higher photocurrent response of STNAs electrode means that, upon the application of a potential bias on the STNAs electrode, the separation and transport efficiency of photogenerated electron/hole pairs is more favorable than that for LTNAs electrode. An increased separation and transport efficiency may contribute positively to the improvement of the PEC performance of STNAs electrode.

Fig. 5b presents the I_{sphd} value of STNAs electrode plotted against the I_{sphd} value of LTNAs electrode in varying concentrations of glucose solution. It was found that the I_{sphd} value of STNAs electrode almost linearly increased with the I_{sphd} value of LTNAs electrode with a slope of $k = 2.08$. That means regardless of whether or not the presence of organic compound (glucose) or different concentration levels, the I_{sphd} value of STNAs electrode was always ~2.08 times as high as that for LTNAs electrode.

Fig. 6a displays a set of voltammograms obtained in a fixed concentration of organic compounds (0.1 M $NaNO_3$ containing 10 mM glucose) under different intensities of UV illumination at the STNAs electrode and the LTNAs electrode (inset), respectively. Under each given light intensity, the photocurrent response increased linearly with biased potential, before leveling off regardless of the electrode materials and the I_{sphd} value of both electrodes increased as the light intensity increased. However, compared with the I_{phd}–E response of LTNAs electrode, the STNAs

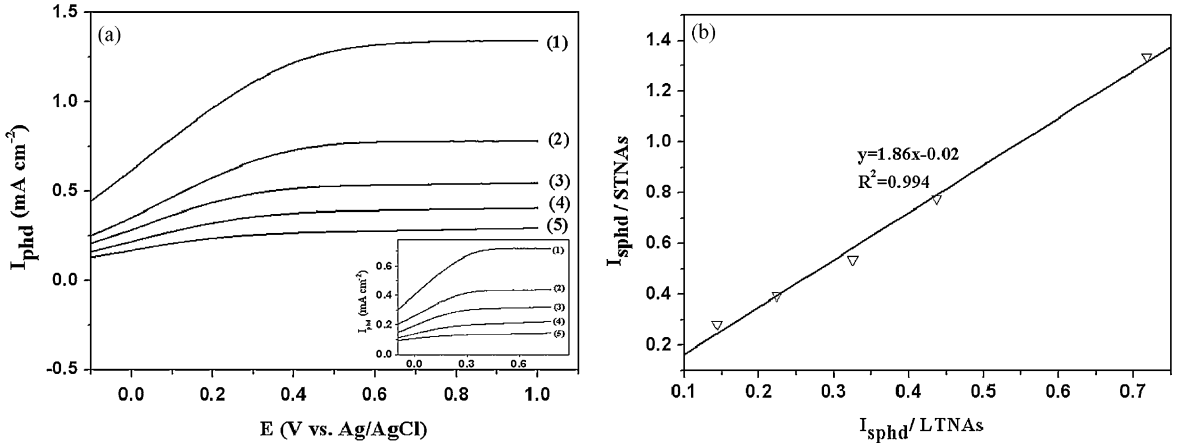

Fig. 6. (a) Voltagrams of STNAs electrode and LTNAs electrode (inset) obtained from a solution containing 0.1 M $NaNO_3$ and 10 mM glucose under illumination of different light intensities. The light intensity: (1) 4.7 mW cm^{-2}, (2) 3.3 mW cm^{-2}, (3) 2.2 mW cm^{-2}, (4) 1.4 mW cm^{-2} and (5) 0.8 mW cm^{-2}. (b) The relationship between the saturated photocurrent density of STNAs electrode and LTNAs electrode at different light intensities.

electrode always displays obviously enhanced photocurrent density at fixed light intensities. The linear response between the I_{sphd} value of STNAs electrode and LTNAs electrode under different UV light intensities were also obtained with a slope of $k = 1.86$, as given in Fig. 6b. Furthermore, the slope obtained here ($k = 1.86$) was close to the above-mentioned slope of I_{sphd}–I_{sphd} ($k = 2.08$), as given in Fig. 5b. The similar value for two kinds of slopes indicates that, either in varying concentrations of glucose solution or under different intensities of UV illumination, the STNAs electrode always reveals obviously enhanced photocurrent response in comparison with the LTNAs electrode, reflecting that the electrons transport inside the STNAs electrode was much more favorable than in the LTNAs electrode. This can be ascribed to the different internal structural morphology of the two electrodes.

3.3. Photoelectrochemical applications

In this work, tetracycline (Figure S4, Supplementary information), as one of typical pharmaceutical and personal care products (PPCPs), was chosen as the target compound [28,29]. PPCPs are a diverse group of environmental chemicals that have received widespread concerns as emerging environmental contaminants as many PPCPs are ubiquitous, persistent and biologically active compounds with recognized endocrine disruption functions [28]. The PEC degradation of tetracycline aqueous was conducted using STNAs electrode and compared with the PEC degradation results obtained using LTNAs electrode. Fig. 7 presents the comparison of the PEC degradation of tetracycline by STNAs electrode and LTNAs electrode. It is evident that the color removal rate and total organic carbon (TOC) removal rate of tetracycline solution reveal similar changing trend for the two electrode materials and the degradation rate of tetracycline on STNAs electrode is much faster than that on LTNAs electrode. This result is in line with the enhanced photocurrent response of the STNAs electrodes, as given in Figs. 4–6. The color removal rate of tetracycline reached 81% for STNAs electrode after 3 h PEC reaction (curve a), which is higher than that attained for LTNAs electrode (60%) under similar conditions (curve b). Within 3 h, 41% of tetracycline was mineralized by STNAs electrode (curve c), while about 23% of tetracycline was mineralized by LTNAs electrode (curve d). That means the PEC oxidation process not only destroys the molecular structure of tetracycline, but also mineralizes part of the organic compound to CO_2 and H_2O. The enhanced PEC performance of STNAs electrode might be attributed to the short nanotubular microstructure, which is considered to be favorable for the highly efficient electron transport inside the electrode. Furthermore, the

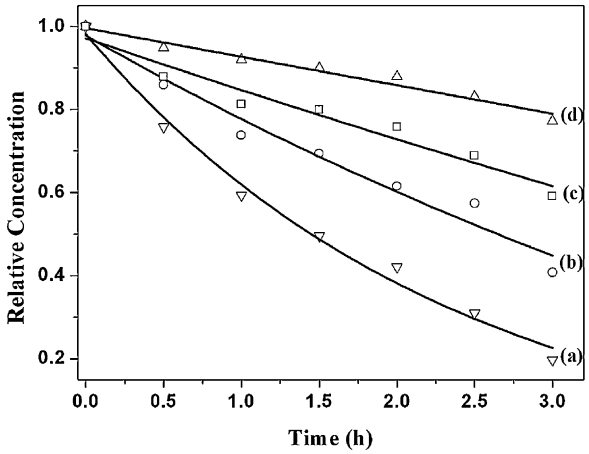

Fig. 7. The variation of absorbance and TOC concentrations of tetracycline solution by the PEC processes of STNAs electrode and LTNAs electrode. (a) Absorbance-STNAs; (b) absorbance-LTNAs; (c) TOC-STNAs; (d) TOC-LTNAs.

bias potential, electrolyte concentration and initial concentration of tetracycline were found to be important factors influencing the PEC process of tetracycline degradation by STNAs electrode (Figures S5–7, Supplementary information).

Compared with the LTNAs electrode, the STNAs electrode prepared by sonoelectrochemical method was robust, with short tube length and thin wall-thickness. Although the STNAs electrode possesses similar roughness factor (surface area) with LTNAs electrode, the special structural characteristic of STNAs electrode may be the main reason for its enhanced photoelectrochemical performance.

The electrochemical (EC), direct photolytic (DP), PC, and PEC processes of tetracycline in aqueous solutions were performed under given conditions on annealed STNAs electrode. In order to quantitatively describe the influence of tetracycline concentration on the reaction kinetics in this work, we apply the pseudo-first-order model, which is usually used to characterize the PEC degradation process of organic compounds. It is evident that the degradation of tetracycline followed the model of Langmuir–Hinshelwood properly. As given in Fig. 8, within 3 h, the EC process was obviously much slower than DP, PC or PEC process. The photolysis of tetracycline, with UV light alone, only results in 14% tetracycline removal after 3 h DP reaction. The presence of TiO_2 nanotubes was proven to be effective and 38% tetracycline was degraded over 3 h. When the STNAs electrode was applied an external anodic potential of +0.5 V, tetracycline removal ratio

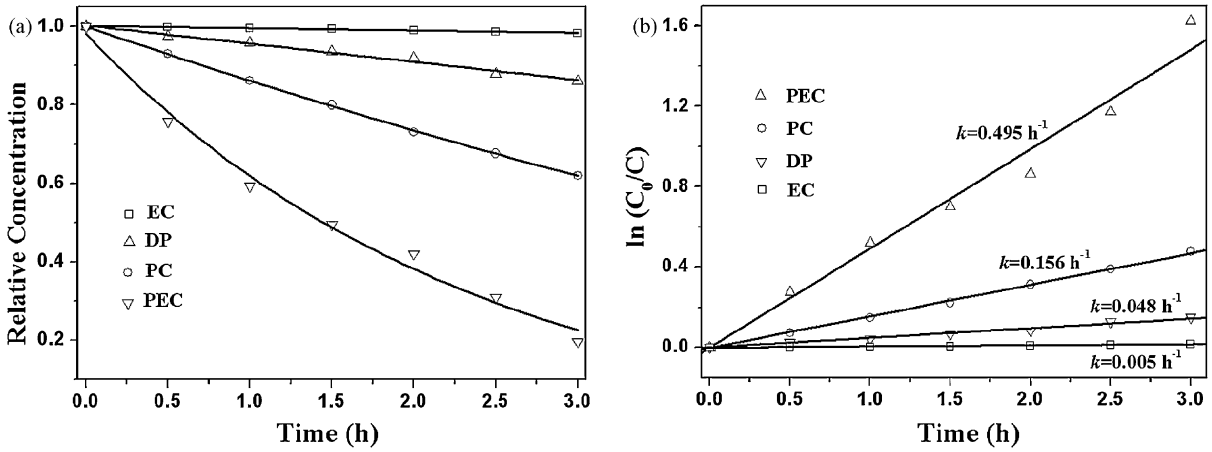

Fig. 8. (a) The electrochemical process, direct photolysis, photocatalysis, and photoelectrocatalysis of solutions of tetracycline by STNAs electrode; (b) the kinetic curves of tetracycline for STNAs electrode in different processes.

sharply increases to 81%. The corresponding reaction rate constant k are ranked as: PEC (0.495 h^{-1}) > PC (0.156 h^{-1}) > DP (0.048 h^{-1}) > EC (0.005 h^{-1}). The obviously enhanced reaction rate constant in PEC process may be ascribed to the suppression of recombination between the photogenerated electron/hole pairs by the external electric field and the kinetic constant of the PEC process by STNAs electrode was ~3.17 times as high as its PC process.

4. Conclusions

The short, robust and highly ordered titania nanotubes were successfully sonoelectrochemically prepared by Ti anodization in HF–H_2O electrolyte solution. Under ultrasonic wave irradiation, the increased mass transfer results in a layer of highly ordered and robust nanotube film with a decreased tube length and wall-thickness. The electron transport process within the STNAs electrode material is much favorable compared with that in the LTNAs electrode prepared with conventional magnetic agitation method, as confirmed by the obviously enhanced photocurrent response of the STNAs electrode. Moreover, the STNAs electrode also reveals improved PEC activity for the color removal and TOC removal of tetracycline solution. The experimental results suggest that the short, robust and highly ordered titania nanotube array electrode serves well as a promising photoelectrocatalyst and may provide an easy and efficient route to remove PPCPs from wastewater.

Acknowledgements

The authors would like to acknowledge the Science and Technology Commission of Shanghai Municipality (08JC1411300, 0952nm01800), the National Nature Science Foundation of China (No. 20677039), the State Key Development Program for Basic Research of China (Grant No. 2009CB220004) and the Program of New Century Excellent Talents in University (No. NCET-04-0406) for financial support.

Appendix A. Supplementary data

Supplementary data associated with this article can be found, in the online version, at doi:10.1016/j.apcatb.2009.08.011.

References

[1] A. Fujishima, K. Honda, Nature 148 (1972) 37–39.
[2] H. Yamashita, H. Nose, Y. Kuwahara, Y. Nishida, S. Yuan, K. Mori, Appl. Catal. A: Gen. 350 (2008) 164–168.
[3] Y. Shimodaira, H. Kato, H. Kobayashi, A. Kudo, J. Phys. Chem. B 110 (2006) 17790–17797.
[4] S. Sakthivel, H. Kisch, Angew. Chem. Int. Ed. 42 (2003) 4908–4911.
[5] V. Zwilling, E. Darque-Ceretti, A. Boutry-Forveille, D. David, M.Y. Perrin, M. Aucouturier, Surf. Interface Anal. 27 (1999) 629–637.
[6] B. O'Regan, M. Gratzel, Nature 353 (1991) 737–739.
[7] Y.X. Li, M. Guo, M. Zhang, X.D. Wang, Mater. Res. Bull. 44 (2009) 1232–1237.
[8] D.W. Gong, C.A. Grimes, O.K. Varghese, W.C. Hu, R.S. Singh, Z. Chen, E.C. Dickey, J. Mater. Res. 16 (2001) 3331–3334.
[9] J.M. Macak, H. Tsuchiya, L. Taveira, S. Aldabergerova, P. Schmuki, Angew. Chem. Int. Ed. 44 (2005) 7463–7465.
[10] M. Paulose, K. Shankar, S. Yoriya, H.E. Prakasam, O.K. Varghese, G.K. Mor, T.A. Latempa, A. Fitzgerald, C.A. Grimes, J. Phys. Chem. B 110 (2006) 16179–16184.
[11] H.E. Prakasam, K. Shankar, M. Paulose, O.K. Varghese, C.A. Grimes, J. Phys. Chem. C 111 (2007) 7235–7241.
[12] Z.Y. Liu, X.T. Zhang, S. Nishimoto, M. Jin, D.A. Tryk, T. Murakami, A. Fujishima, J. Phys. Chem. C 112 (2008) 253–259.
[13] C.A. Grimes, J. Mater. Chem. 17 (2007) 1451–1457.
[14] Z.H. Zhang, Y. Yuan, G.Y. Shi, Y.J. Fang, L.H. Liang, H.C. Ding, L.T. Jin, Environ. Sci. Technol. 41 (2007) 6259–6263.
[15] X. Quan, S.G. Yang, X.L. Ruan, H.M. Zhao, Environ. Sci. Technol. 39 (2005) 3770–3775.
[16] G.K. Mor, O.K. Varghese, M. Paulosea, K. Shankara, C.A. Grimes, Sol. Energy Mater. Sol. Cells 90 (2006) 2011–2075.
[17] Y.B. Liu, B.X. Zhou, B.T. Xiong, J. Bai, L.H. Li, Chin. Sci. Bull. 52 (2007) 1585–1589.
[18] Q. Zheng, B.X. Zhou, J. Bai, L.H. Li, Z.J. Jin, J.L. Zhang, J.H. Li, Y.B. Liu, W.M. Cai, X.Y. Zhu, Adv. Mater. 20 (2008) 1044–1049.
[19] J.L. Zhang, B.X. Zhou, Q. Zheng, J.H. Li, J. Bai, Y.B. Liu, W.M. Cai, Water Res. 43 (2009) 1986–1992.
[20] S. Yoriya, M. Paulose, O.K. Varghese, G.K. Mor, C.A. Grimes, J. Phys. Chem. C 111 (2007) 13770–13776.
[21] Y.S. Sohn, Y.R. Smith, M. Misra, V. Subramanian, Appl. Catal. B: Environ. 84 (2008) 372–378.
[22] S.K. Mohapatra, M. Misra, V.K. Mahajan, K.S. Raja, J. Catal. 246 (2007) 362–369.
[23] J. Bai, B.X. Zhou, L.H. Li, Y.B. Liu, Q. Zheng, J.H. Shao, X.Y. Zhu, W.M. Cai, J.S. Liao, L.X. Zou, J. Mater. Sci. 43 (2008) 1880–1884.
[24] K. Shankar, G.K. Mor, H.E. Prakasam, S. Yoriya, M. Paulose, O.K. Varghese, C.A. Grimes, Nanotechnology 18 (2007) 065707.
[25] N.K. Allam, C.A. Grimes, Sol. Energy Mater. Sol. Cells 92 (2008) 1468–1475.
[26] Y.B. Liu, B.X. Zhou, J. Bai, J.H. Li, J.L. Zhang, Q. Zheng, X.Y. Zhu, W.M. Cai, Appl. Catal. B: Environ. 89 (2009) 142–148.
[27] D.L. Jiang, H.J. Zhao, S.Q. Zhang, R. John, J. Catal. 233 (2004) 212–220.
[28] S.J. Jiao, S.R. Zheng, D.Q. Yin, L.H. Wang, L.Y. Chen, Chemosphere 73 (2008) 377–382.
[29] O.K. Dalrymple, D.H. Yeh, M.A. Trotz, J. Chem. Technol. Biotechnol. 82 (2007) 121–134.